Int. J. Heat Mass Transfer. Vol. 24, No. 5, pp. 919–931, 1981
Printed in Great Britain

0017–9310/81/050919–13 $02.00/0
Pergamon Press Ltd

LAMINAR STARTING PLUME TEMPERATURE FIELD MEASUREMENT

D. J. SHLIEN* and RAYMOND L. BOXMAN
School of Engineering, Tel Aviv University, Tel Aviv, Israel

(*Received* 17 *July* 1979 *and in revised form* 3 *September* 1980)

Abstract—The temperature field of an axisymmetric laminar starting plume was measured for the first time, using an interferometric measurement technique and Abel inversion data reduction. The measurements revealed that the column of buoyant fluid following the cap has almost the same temperature distribution as the steady plume, confirming an aspect of Turner's model of the starting plume cap for the laminar case. Besides the temperature peak on the axis corresponding to the steady plume peak, an off-axial peak in the middle of the cap and an unexpected axial peak near the cap leading edge were observed. The former peak is a result of the entrained ambient fluid while the latter is unexplained but is probably associated with the instability previously observed. Temperature gradients near this peak, are estimated to be as high as 20 C°/mm.

NOMENCLATURE

- D, thermal diffusivity;
- l, diffusion length scale;
- p, rate of heat injection;
- Pr, Prandtl number, ratio of diffusivities of momentum to heat;
- Q_m, total measured heat content of starting plume cap;
- Q_T, estimate of total heat content of starting plume cap using Turner's model;
- r, radial distance from symmetry axis;
- r_0, $= r$ of the off-axial temperature peak;
- t, time measured from initial injection;
- T, temperature above ambient;
- T_0, average cap temperature above ambient;
- v_a, fluid velocity on symmetry axis at the base of the cap;
- v_c, starting plume cap gross convection velocity;
- v_p, steady plume gross convection velocity;
- z, vertical distance measured from the source position.

Greek symbols

- τ_c, convection time for the entrained ambient fluid to be carried from the cap base to the cap leading edge;
- τ_D, a diffusion time scale;
- τ_0, convection time for the fluid element located at the spiral center;
- τ_r, time required for one revolution of the spiral.

INTRODUCTION

SOME fundamental phenomena in natural convection heat transfer are those resulting from the release of buoyancy from a point source into a quiescent unstratified fluid. The phenomena can be classified according to the time dependence of the buoyancy injection: the thermal for pulse injected buoyancy, the steady plume for continuous buoyancy injection and the starting plume which results from the initiation and then continued buoyancy injection. Here we are concerned with the latter phenomenon.

Structures similar to the starting plume cap have been observed in melting and freezing processes, and in heat transfer from a rigid body to a fluid over a considerable Rayleigh number range. Thus, besides being of fundamental interest, understanding the starting plume cap may be helpful in furthering our understanding and possibly aiding the enhancement of more practical heat transfer problems. Also knowledge of the starting plume cap can be applied to understanding aspects of the thermal and vortex rings.

Turner [1] was the first to study the phenomenon which he named the starting plume. He was concerned with the turbulent case which is important for cloud convection studies. As a result of his observations he suggested a model of the starting plume consisting of a steady plume capped by a thermal whose buoyancy increases as a result of the slower upward convection velocity of the cap as compared with the steady plume below it. His measurements confirmed some aspects of the model.

The first observations of the laminar starting plume were obtained using shadowgraph techniques [2]. A sample shadowgraph photo is presented in Fig. 1 in which the spiral of fluid characteristic of vortex rings can just be distinguished. The cap convection velocity and the ratio of diameter to height (aspect ratio) were measured. The cap velocity was found constant over the entire observation time but the aspect ratio required a short development time before becoming constant. However, by a proper choice of apparent starting time the aspect ratio could be made constant for essentially the entire observation time of 6 s. Measurements of other overall dimensions of the cap shadowgraph also indicated geometrical similarity.

* Present address: Department of Mechanical Engineering, University of Houston, Houston, TX 77004, U.S.A.

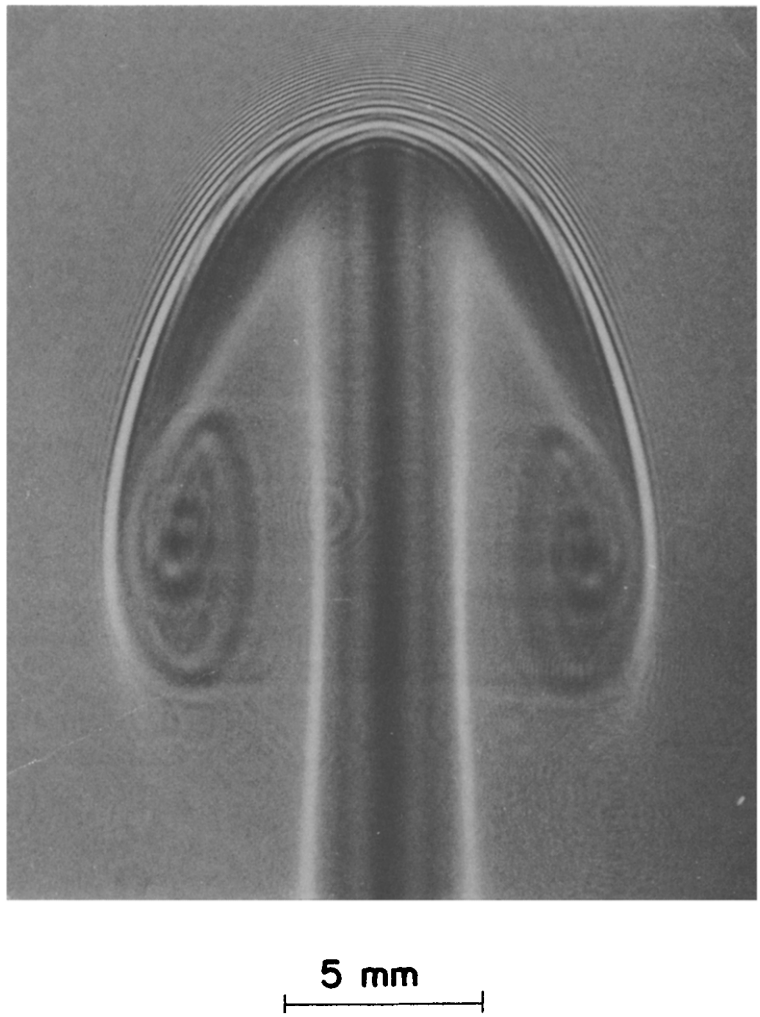

FIG. 1. Shadowgraph of the starting plume cap rising at a velocity of 12 mm/s in a concentrated sodium carbonate solution (Prandtl number $\cong$ 21). The leading edge is 80 mm above the electrode which is injecting heat at 1.0 cal/s. The spiral which is clearly visible here is not visible when 0.1% $NaCl/H_2O$ ($Pr = 7$) is used as the test medium.

The buoyancy was injected in the form of heat at a rate of 1.0 cal/s, resulting in a cap velocity of 12 mm/s and an aspect ratio of 0.2. Turner's [1] model was applied to this case and was found to describe the cap motion well.

No velocity field measurements of the cap have been reported; however the particle path element (tracer streak) field of the thermal [3] presented in Fig. 2 should qualitatively resemble the starting plume cap velocity field. In the case of the cap, buoyant fluid is convected up through the base center (at higher velocities than in the thermal) while for the ideal thermal, ambient fluid is entrained through the base. The thermal shown in this figure is somewhat less than ideal, having a trailing region of buoyant fluid released after the thermal. This photograph will be used to help interpret the temperature field measurements of the starting plume cap.

In the present work, the temperature field of a laminar axisymmetric starting plume will be presented and discussed after a brief discussion of the apparatus and measurement technique. Predominant features include an axial column similar to the steady plume, an off-axial temperature peak, and an unexpected temperature peak on the axis near the cap's leading edge. The above features will be interpreted in light of Turner's model, previously described measurements in other buoyant phenomena, and vortex ring studies. Several unanswered questions will be pointed out, and directions for further research will be indicated.

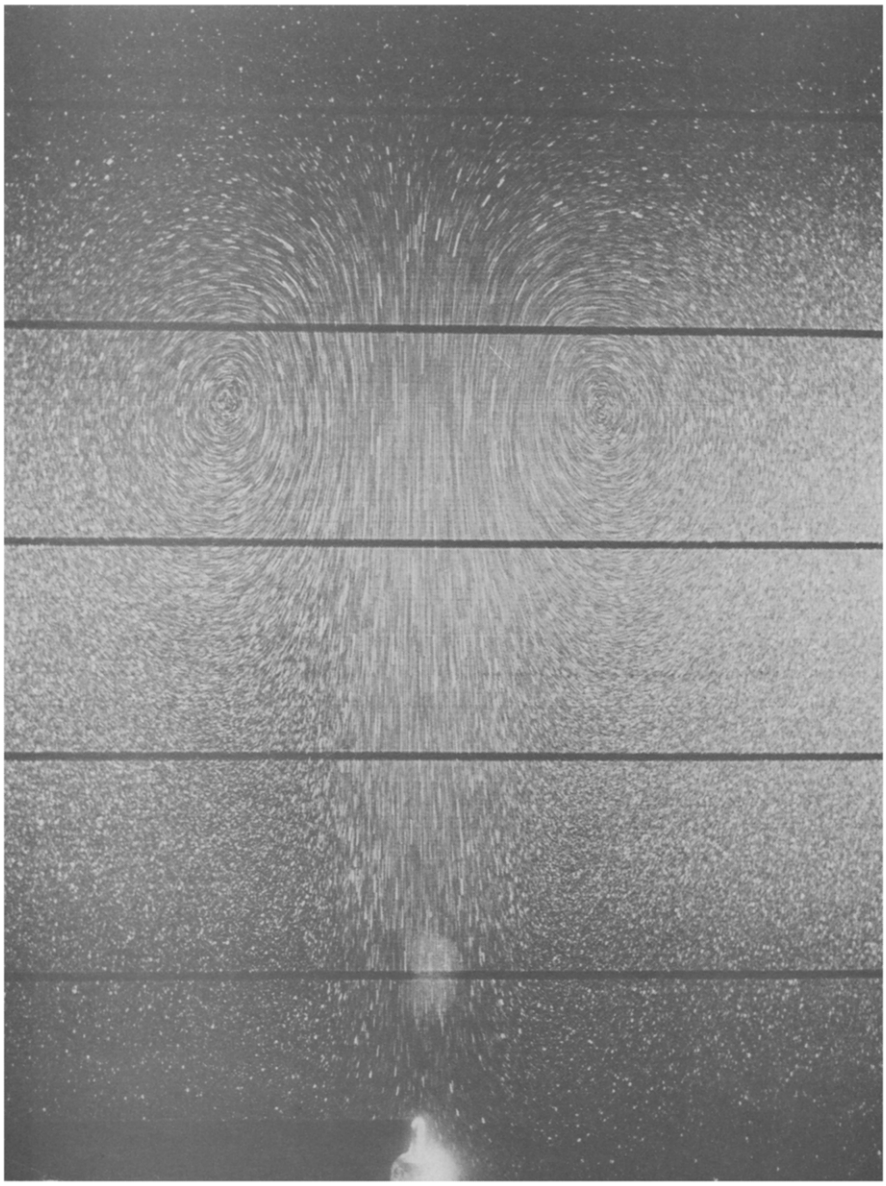

FIG. 2. Streak photo of a laminar thermal at a height of 70 mm from the electrode, rising at a velocity of 1 mm/s with a total of 0.7 cal of heat injected (effective Rayleigh number = 1.4×10^4). Lighting is by a 1 mm thick vertical light sheet through the electrode axis. The dark horizontal lines are 20 mm apart. The streaks result from a time exposure of the paths of small tracer particles.

APPARATUS AND MEASUREMENT TECHNIQUE

The test medium, a 0.1% $NaCl/H_2O$ solution, is contained in a 200 × 200 × 300 mm high glass aquarium V, Fig. 3. Heat is injected into the solution at a rate of 6.1 cal/s by direct ohmic heating of the liquid near a small conical graphite electrode e of half angle of 15° and base 5 mm dia. supported at the center of a large horizontal acrylic plastic plate. This heating is achieved by imposing an AC voltage of 5 kHz frequency between the conical electrode and four much larger electrodes E situated in the solution at the corners of the aquarium. Since the current density is much larger near the smaller electrode than the large ones, only the fluid near the conical electrode is appreciably heated. Further details on the injection technique may be found in [4].

The temperature field was measured with the aid of a Mach–Zender interferometer as described in [1]. A

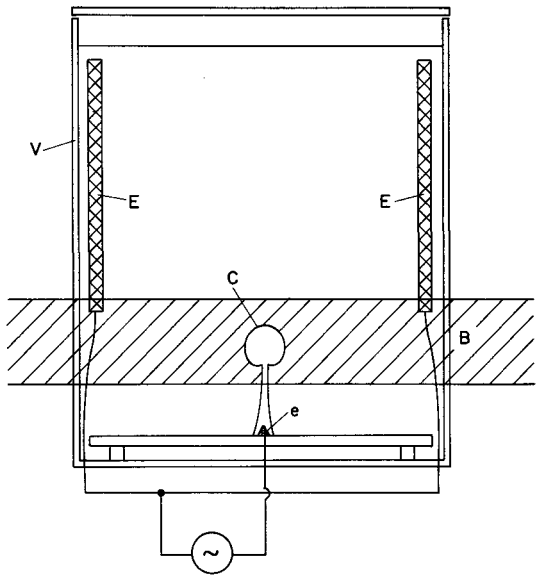

FIG. 3. Schematic of apparatus. Dilute salt solution is contained in the vessel V. Electric current of frequency 5 kHz, is conducted from the small electrode e, to the four large ones E located in the vessel corners. The laser beam B, a leg of the Mach–Zender interferometer passes through the starting plume cap C.

typical interferogram was chosen for detailed analysis and is shown in Fig. 4. A maximum of only eight fringes is observed requiring the measurement of fractional fringe shifts in order to obtain reasonable accuracy. (It should be noted that because of the axial, rather than two-dimensional, symmetry the fringes do not represent constant temperature contours.) The temperature field of the cap is deduced from the interferogram using the following procedure [5]. Various sections of the interferogram negative are scanned with a microdensitometer in the direction normal to the axis of symmetry. For each section the fringe shift was computed from the measured optical density as described in [5]. The Bockasten series approximation of the Abel integral was used with the fringe shift data of each section to obtain the radial refractive index variation for each section. In this approximation a finite number (in this case 20) of evenly spaced points are chosen for analysis. Thus the spatial resolution is limited by the spacing between these points, in this case 0.3 mm. Finally, using refractive index variation with temperature data measured for the same salt solution [6], temperature profiles for each section were computed.

Three representative temperature profiles are presented in Fig. 5 (lower, middle and upper sections). Error bars on the mean curves indicate the error resulting from 'noise' on the microdensitometer output. The left-hand and right-hand sides were analyzed independently to show deviations stemming from the lack of symmetry of the cap which can be seen in the interferogram (Fig. 4). The symmetry is excellent in the lower portions of the cap but appears to worsen progressively with height. The overall degree of asymmetry is acceptable, especially considering difficulties with alternative measurement techniques in the light of the low temperature difference range and high spatial resolution requirements. Temperature profiles to be presented in the following section will be the average over left and right hand sides.

OBSERVATIONS

The measured temperature field is presented in two ways: (a) as a series of radial temperature profiles (Fig. 6) to indicate the development with height of the radial temperature distribution; and (b) as contours of constant temperature (Fig. 7) to show the entire temperature field. In both figures the spatial coordinates have been normalized with the radius of the off-axial temperature peak, $r_0 = 4.1$ mm while temperatures have been normalized by an average cap temperature above ambient, $T_0 = 3.36\,C°$. This average was taken over the volume inside the $0.1\,C°$ temperature contour starting from the cap base taken as height $z = 14.6\,r_0$. The cap base position was chosen close to the neck of the plot of the heat residing at a section per unit height as a function of the height (to be presented subsequently). Thus if temperature field similarity does exist, the plotted curves should be of a universal nature.

Rather large radial temperature gradients are obtained, as can be observed in temperature profile K (Figs. 6 and 7). The slope $\partial T/\partial r$ of the almost linear region near the axis and of the outer region is essentially the same, $-4.4\,C°$/mm. In the intermediate region $0.5\,r_0 < r < r_0$, the slope is $2.6\,C°$/mm. Very large axial temperature gradients are also observed in the vicinity of the leading edge. While an accurate assessment of this gradient is not possible because of the measurement technique used, the gradient may be estimated to be of the order of $\partial T/\partial z = -20.0\,C°$/mm. Features of the starting plume temperature field which will subsequently be discussed include the temperature profile at lower heights $z < 14\,r_0$, the off-axial temperature peak at coordinates $(z/r_0, r/r_0)$ of (15.8, 1.0), the axial temperature peak near the leading edge at (17.8, 0), and the valley region (local temperature minimum) in the region $14.5 < z/r_0 < 16.5$ and $0.3 < r/r_0 < 0.7$.

DISCUSSION

1. *Data comparison with starting plume model*

Turner's [1] model of the starting plume consists of a steady plume topped by a thermal of increasing buoyancy. Here the data will be examined to see to what extent the model conforms to the actual starting plume. This will be accomplished by comparing the temperature profiles measured at the lower sections with those corresponding to the true (undisturbed by the cap) steady plume. Since there are no measurements of the laminar thermal temperature field, the cap temperature field cannot be compared with that of the former. However, the measured total heat content of the cap will be compared with that estimated from the model.

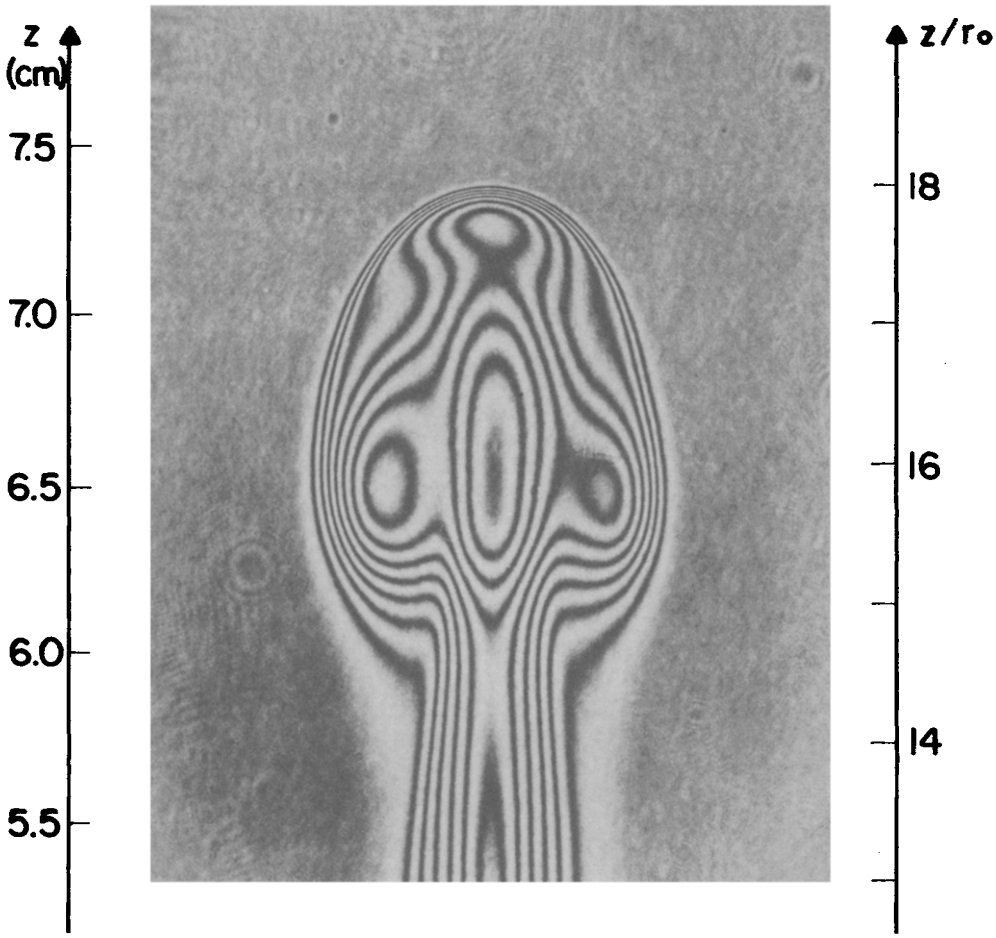

FIG. 4. Interferogram of the starting plume cap analyzed here. Test medium is 0.1% sodium chloride solution ($Pr = 7$)., injection rate is 6.1 cal/s and the rise rate is 25 mm/sec. It should be noted that the fringes are not equithermal lines. Vertical scales are the height above the electrode base, in cm (left side) and normalized (right side).

Qualitatively, it can be seen immediately from Fig. 6 that the temperature profiles at the lowest sections (such as A and C) are similar to the steady plume profile (bell-shaped). Furthermore, it may be observed that except for the outer region, the profile shape remains almost unchanged close to the cap center (profile K). In Fig. 8 a comparison is presented between the cap profile (section B) and the steady plume profile at the same height obtained from an interferogram photographed 10 s* after the cap has passed. The error bars on the two curves in Fig. 8 indicate the spread between the right and left hand side data. A comparison may also be made with Fujii's [8] analytical solution for the steady plume, if the concept of an apparent origin is used to account for the finite source dimensions. An apparent source distance of 281 mm is obtained through a best fit of Fujii's solution to the high accuracy portion of the steady plume measurement, as described in [7]. As may be determined from Fig. 8, the maximum deviation between the true steady plume profile and the starting plume profile near the base is less than 9% of the axial temperature. As z is increased, the steady plume profile remains essentially constant within the region of the cap due to the large distance from the apparent source compared with the cap height. The cap profile in the vicinity of the axis ($r < 0.5\,r_0$) shows increasing deviation from the steady plume profile, reaching a deviation of 18% of the plume axial temperature at the cap center ($z = 15.8\,r_0$).

Thus it may be concluded that the starting plume below the cap base is essentially a steady plume. As the profiles are examined at successively higher distances within the cap, the temperature profiles (and thus

* Previous studies [7] have shown that steady-state is obtained within 5 s after the passage of the cap. Nevertheless this was checked by comparing the 10 s profile with one obtained 20 s after cap passage; the two profiles agreed within the experimental error.

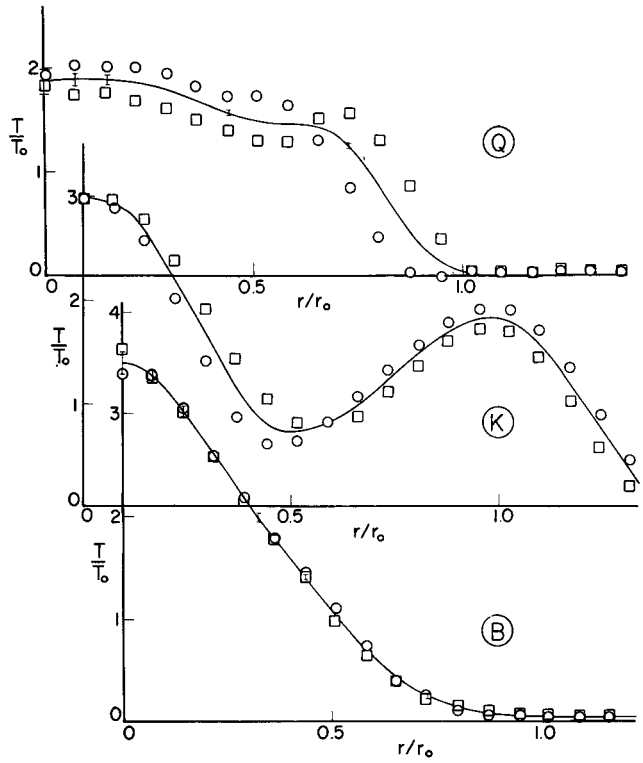

FIG. 5. Typical starting plume temperature profiles near the cap base (B), the center (K), and top (Q) of the cap. The faired curve represents an average between the data of the left-hand side (○) and right-hand side (□) from the interferogram each analyzed independently. Error bars indicate the error resulting from 'noise' on the microdensitometer output. The temperature is normalized with the average cap temperature above ambient, $T_0 = 3.36\,C^\circ$ and the radius is normalized to the radius of the off-axial peak, $r_0 = 4.1$ mm.

probably the velocity profiles) deviate from those of the steady plume starting with the outer regions (the tails) of the profiles, while the steady plume profiles persist near the axis. At the cap center, the temperature profile is still similar to that of the steady plume up to $r \cong r_0/2$.

The normalized heat content per unit height is plotted (Fig. 9) to show how the heat content at a horizontal section changes with height. It can be seen that the greatest amount of heat is contained in the section of the off-axial temperature peak where the cap is widest. The dashed horizontal line indicates the height assumed to be the cap base used in the calculation of the total heat content of the cap, Q_m. Also in this figure, the normalized heat content per unit height of the steady plume measured after the passage of the cap at the same height as section B is indicated with an asterisk. This integrated heat content is almost the same as that at the same height for the starting plume. This together with the result of the preceding paragraph represents a confirmation of the applicability of Turner's model [1] to the laminar case.

It is to be noted that the Fig. 9 data are sensitive to the tail region of the temperature profiles where the temperature is low and thus of poorer accuracy. The curve of Fig. 9 was integrated in the cap region ($z \geqq 14.6\,r_0$) to give the cap total heat content, $Q_m = 3.8$ cal. Turner's model results in $Q_T = p(1 - v_c/v_p)t$ where Q_T is the total heat contained by the cap, p is the rate of the heat injection and v_c and v_p are the cap and steady plume gross convection velocities such that the ratio $v_c/v_p \cong 0.52$. For the case presented here, $Q_T = 7.6$ cal, a deviation by a factor of two. The large discrepancy between Q_m and Q_T is believed to be caused primarily by heat conduction to the electrode. Inaccuracies in the temperature measurement, especially far from the axis, and inaccuracies in the determination of the v_c/v_p ratio are expected to play a secondary effect.

2. *Off-axial valley and peak*

To explain the off-axial temperature minimum and peak (sections I–N, Figs. 6 and 7) characteristics of the velocity field will be used. Thus a brief description of velocity field is first presented here. The velocity field is

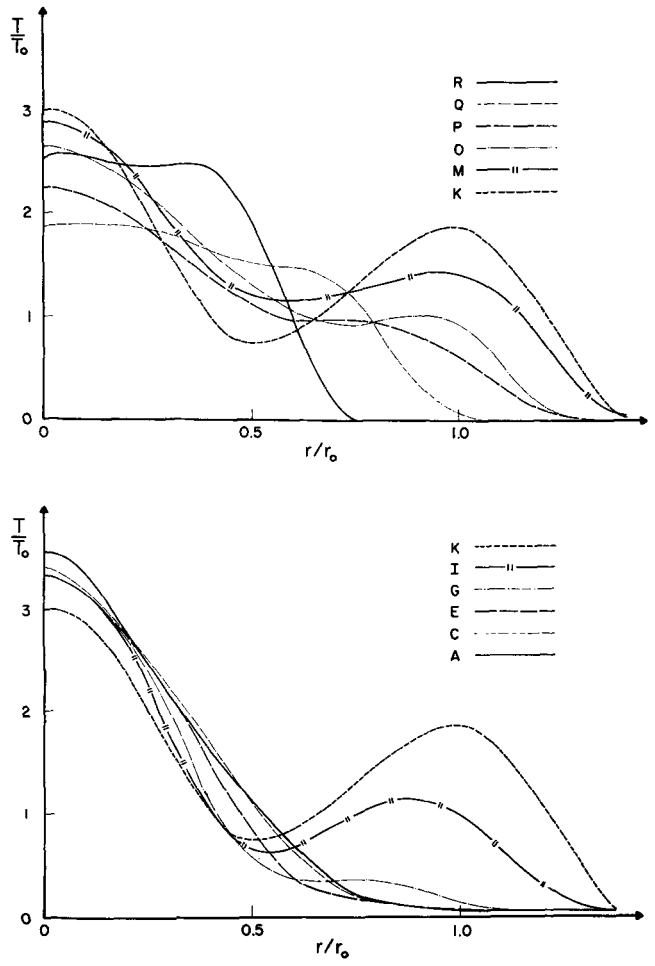

FIG. 6. Superposed temperature profiles in the lower half (lower plot) and upper half of the starting plume cap. Section locations are shown in Fig. 7.

qualitatively the same as that of the thermal, indicated in Fig. 2 by the tracer particle streaks. Since the fluid temperature in the wake of the thermal is considerably less than that in the thermal body while the fluid temperature in the steady plume portion of the starting plume is larger than that of the cap, the main difference between the cases of the thermal and the cap is that the velocity in the steady plume region relative to the cap should be larger than that depicted in Fig. 2 for the thermal. The fluid in the steady plume rises from the source and decelerates rapidly once it enters the cap. It continues to rise and decelerate inside the cap until it reaches the region of the cap leading edge (stagnation region) where it deflects outwards. Relative to the upward moving cap, the fluid then falls downward forming a vortex ring velocity pattern. At the base of the cap just outside the region where the steady plume joins the cap, ambient fluid is entrained into the cap. It is this entrained ambient fluid which results in the off-axial minimum in the temperature field.

The entrained ambient fluid results in the spiral which is just visible in the cap shadowgraph of Fig. 1. This type of spiral is much clearer in the non-buoyant vortex ring photo (Fig. 10). In this photo, dyed (white) fluid is injected from a jet into an ambient transparent fluid (appearing dark in the photograph). The dyed fluid spirals together with a layer of ambient fluid towards what must be the rotational center in the convecting frame. The dyed fluid which originates in the jet, is analogous with the heated fluid originating near the electrode in the cap experiment. It is apparent that ambient fluid is entrained into the vortex at point P in Fig. 10. By analogy, it may be expected that ambient fluid is entrained in the region of the point (14.3, 1.0) in the cap of Fig. 7. An idea of how this entrainment takes place in the cap may be obtained from the streak photo (Fig. 2), but the reader is reminded that the centers of rotation seen in the photo are points of zero velocity while the vortex ring (or cap) rotational centers are convecting upward.

It is the entrained ambient fluid which is responsible

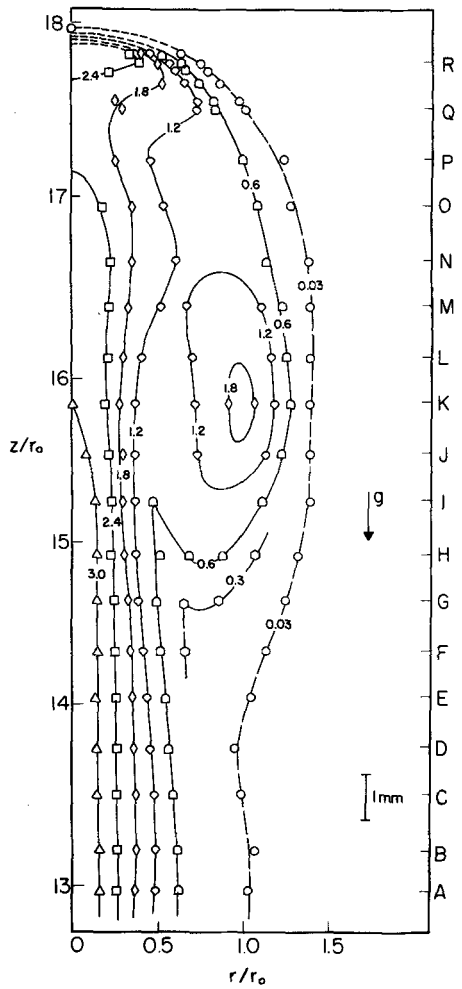

FIG. 7. Temperature field contours interpolated from the temperature profiles.

for the valley region of the temperature contours. The fluid in the entrainment region is near ambient temperature, as expected. As the fluid is convected up towards the valley region thermal diffusion takes place and the entrained fluid is thus heated. Rough estimates (see Appendix) indicate that the convection time and thermal diffusion time are of the same order of magnitude and thus an accurate prediction of the valley temperature can be made only with the aid of a more complete analysis. The temperature in the valley region was measured to be $0.6\ T_0$.

The dye forming the spiral of the vortex ring diffuses relatively slowly into the ambient fluid (i.e. the Prandtl number is very high) and thus many rotations can be seen. As many as twenty rotations can be found in the beautiful photo of a smoke-in-air (also having a very high effective Prandtl number) vortex ring in [10]. For heat in water, the Prandtl number 7 is considerably smaller than for the dye-in-water and smoke-in-air cases and thus the diffusion process takes place more rapidly. A crude estimate of the number of warm-cool layers that should be present in the cap under investigation was made by comparing the upward convection time with the rotation time (see Appendix); 2.6 are estimated. For the spiral center region, the thermal diffusion time is estimated to be considerably shorter than the convection time and thus the temperature distribution in this region should be diffused, as observed in the present experiment. It should be noted, however, that spatial resolution limitations of the Bockasten finite series approximation to the Abel integral would prevent detection of weak vestigial spiral layers.

The off-axial temperature peak may be explained as follows. The fluid in the vicinity of the off-axial peak originated near the heat source, and thus is relatively

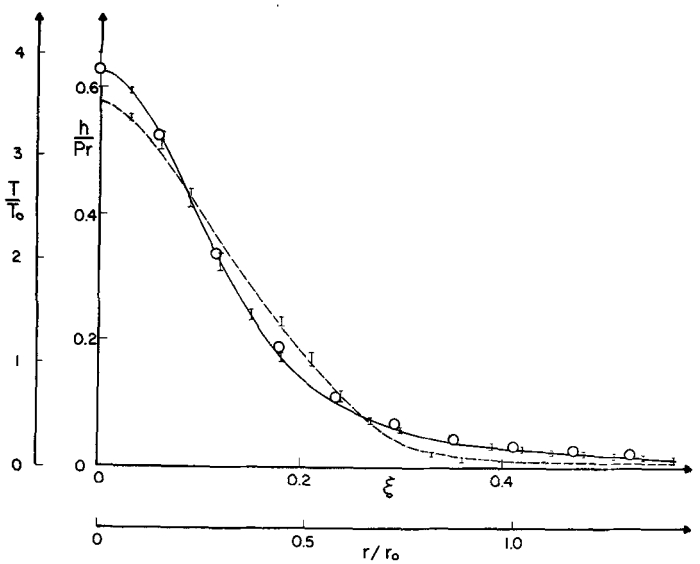

FIG. 8. The temperature profile at section B of the starting plume (broken line) compared with that measured of the steady plume at the same height (solid line) and with an analytic solution [8] (circles) for the steady plume. The inner coordinates correspond to those used in the analytic solution, [8]. Error bars indicate the spread between left- and right-hand side data.

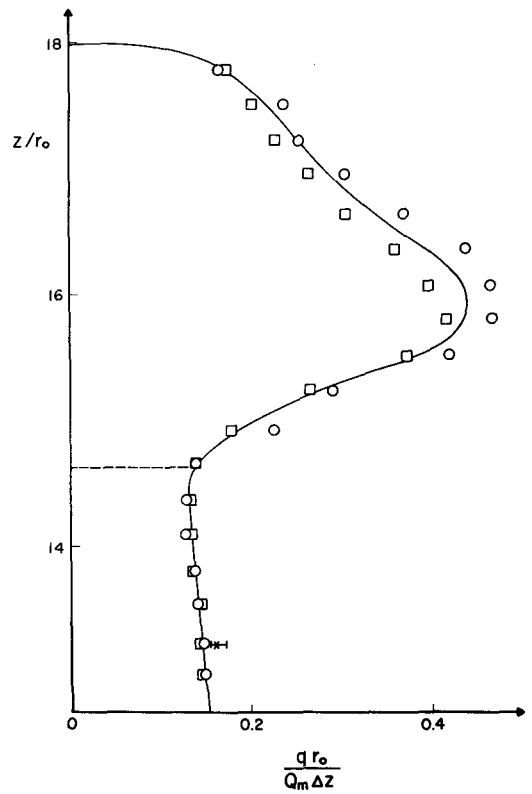

FIG. 9. Heat content per unit height $q/\Delta z$ normalized by Q_m/r_0 as a function of normalized height where Q_m is the measured total heat content above the broken line. The asterisk datum point is for a steady plume at the same height (equivalent to height of section B, Fig. 7).

warm while the fluid in the valley region contains entrained ambient fluid and thus is relatively cool. The off-axial peak can exist only if the heat is slow in diffusing away, i.e. if the Prandtl number is high. This is well illustrated in Fox's numerical solution of the governing equations [11] for the thermal. For $Pr = 0.25$ the temperature peak is on the axis, whereas for $Pr = 2$ the temperature peak is off the axis. It may be noted that no evidence of a spiral structure was observed in Fox's results, possibly because of the coarse grid that was necessary for reasonable computation time.

3. *Axial peak*

The temperature peak at (17.8, 0) is unexpected and thus most interesting. Since its temperature is larger than that of the fluid in its neighborhood, it must have originated when the cap was located at a lower position and thus the temperature of the entraining hot fluid was hotter. As the cap rises the fluid temperature at the peak location must decrease more slowly than the fluid in its neighborhood, possibly because of its closer proximity to the stagnation point in the convecting frame. In fact, it is suspected that its temperature relative to its surroundings continually increases until the fluid at this peak temperature breaks away from the remainder of the cap. It is this breaking away that may cause the instability or 'transition' described in [12]. The slight lack of symmetry in the interferogram may be caused by the cap being in the initial stages of this 'transition.' The empirical criterion for the instability given in the reference is that $pt = 19$ cal while here $pt = 18$ cal where p is the rate of heat injection. Later stages of this 'transition' can be seen in the interferograms of Fig. 11.

SUMMARY AND CONCLUSIONS

These measurements, the first measurements of the temperature field of the starting plume, revealed some interesting features while also raising some equally interesting questions. The radial temperature profile of the column of buoyant (warm) fluid below the cap base was close to that of the steady plume. The axial region of the temperature profile did not change greatly up to the cap center ($z = 15.8\, r_0$). An off-axial temperature peak was observed at the height of the cap center at dimensionless coordinates $(z/r_0, r/r_0) = (15.8, 1.0)$ while an unexpected temperature peak was also observed on the axis near the leading edge at height $z = 17.8\, r_0$. The temperature gradients were large, considering the absence of a rigid body in the field; the maximum radial gradient being 4.4 C°/mm while the maximum axial gradient was approximately 20.0 C°/mm at the cap leading edge. It is to be noted that these gradients may actually be higher since measurement resolution limitations tend to reduce the apparent gradients.

These measurements confirm one aspect of Turner's [1] model of the starting plume cap, viz. the temperature profile of the column of fluid below the cap base is very close to that of a steady plume. Ambient fluid is entrained from a region at the cap base just outside the steady plume region. It is due to this entraining fluid that the off-axial temperature peaks are observed. The axial temperature peak near the leading edge is thought to be associated with the instability of the cap, previously observed [12].

No evidence of a spiral structure was observed at the Prandtl number of the present experiment, 7.1, in contrast with observations of the higher Prandtl number starting plume cap [4] or the dyed vortex ring [9]. The lack of the spiral structure is probably due to the characteristic diffusion time being considerably less than the convection time in the region near the spiral center.

New questions raised are as follows: How does the axial peak near the leading edge develop with time? Does its development contradict the normally assumed similarity of the temperature field? How do the off-axial temperature peaks develop? What is the effect of the Prandtl number of the starting plume? Further measurements are required to answer these questions. Measurements of the time development of the temperature field, refinement of the temperature field measurement technique, measurements of the velocity field, and simultaneous measurements of the tempera-

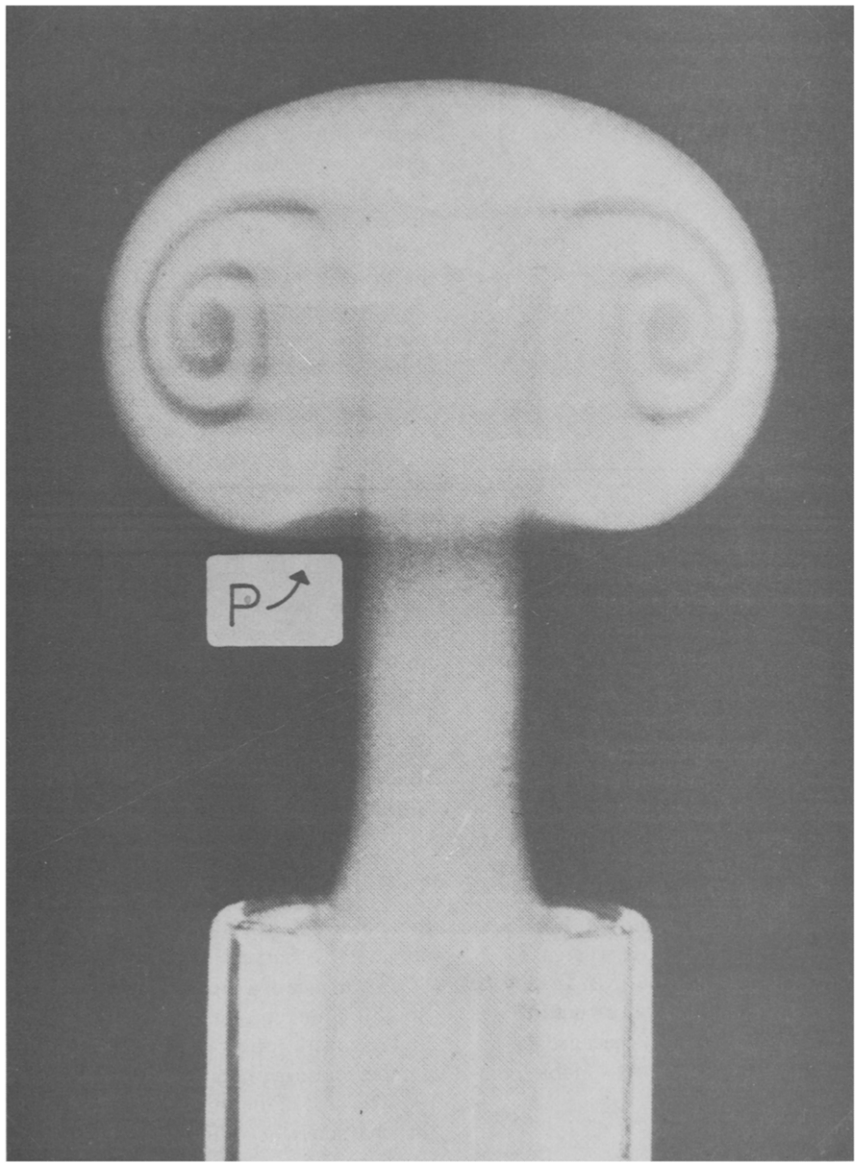

FIG. 10. Non-buoyant vortex ring dye photograph from [9]. This is one of a time sequence shown in the reference. Point P indicates where ambient fluid is being entrained.

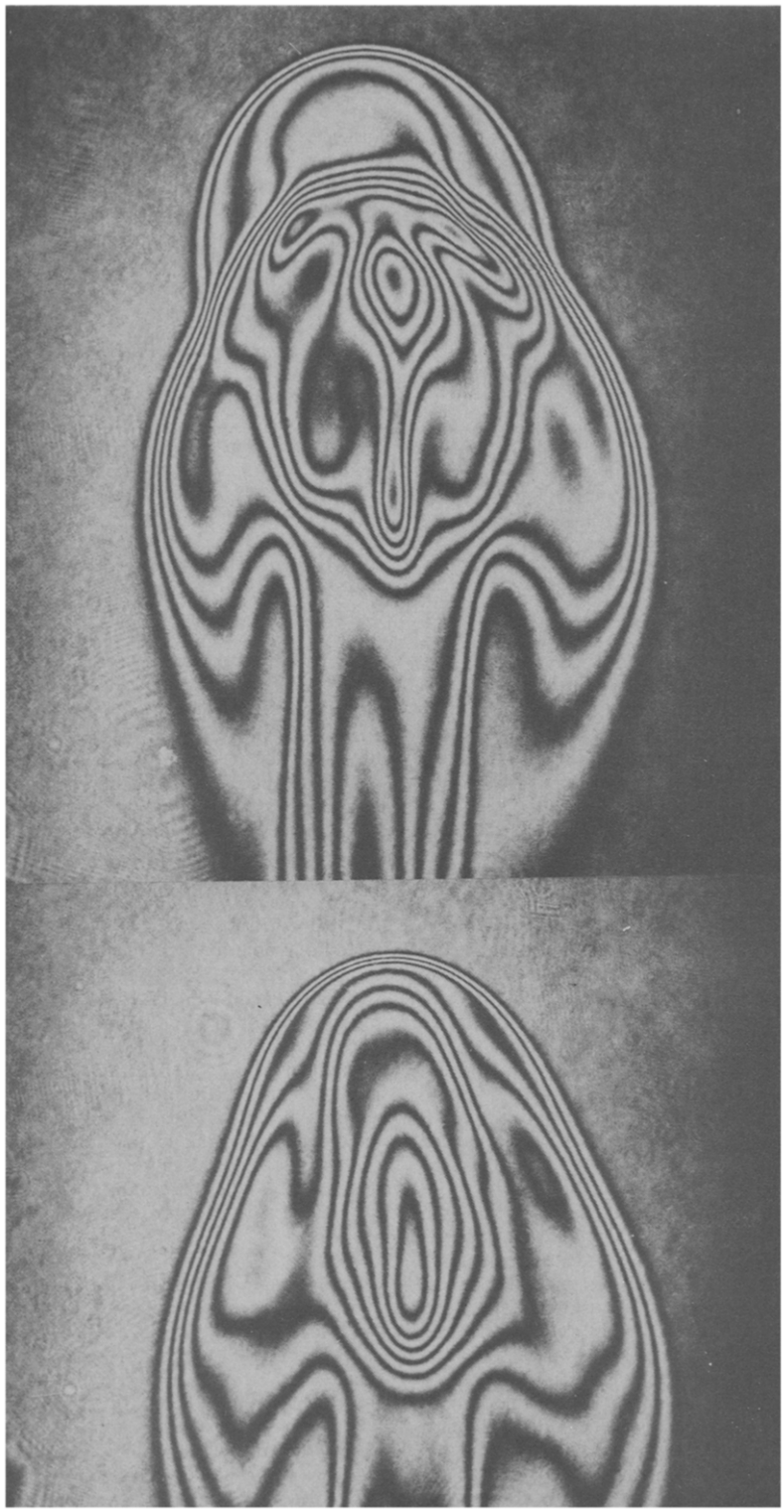

FIG. 11. Sequential interferograms of the instability of the starting plume cap. The lower photo was taken approximately 0.3 s before the upper one. Height of the leading edge above the electrode in the lower photo is 116 mm while in the upper one is 124 mm. Heat injection rate p was 6.0 cal/s and upward convection velocity 25 mm/s. Test medium is the same as for the experiment reported here.

ture and velocity fields should help resolve these questions.

Acknowledgements—The authors gratefully acknowledge the data reduction assistance of B. Jordan and D. Cohen.

REFERENCES

1. J. S. Turner, *J. Fluid Mech.* **13,** 356 (1962).
2. D. J. Shlien, *Physics Fluids* **19,** 1089 (1976).
3. D. J. Shlien and A. Brosh, *Physics Fluids* **22,** 1044 (1979).
4. D. J. Shlien, *Rev. Sci. Instrum.* **48,** 1152 (1977).
5. R. L. Boxman and D. J. Shlien, *Appl. Opt.* **17,** 2788 (1978).
6. R. L. Boxman and D. J. Shlien, *Rev. Sci. Instrum.* **49,** 861 (1978).
7. D. J. Shlien and R. L. Boxman, *Physics Fluids* **22,** 631 (1979).
8. T. Fujii, *Int. J. Heat Mass Transfer* **6,** 592 (1963).
9. J. Okabe and S. Inoue, Report of Research Institute of Applied Mechanics, Kyushu University **8,** 91 (1960). Photographs referred to are reproduced in Fig. 7.22, plate 20 of G. K. Batchelor, *Fluid Dynamics*. Cambridge University Press, Cambridge (1970).
10. R. H. Magarvey and C. S. MacLatchy, *Canad. J. Phys.* **42,** 678 (1964).
11. D. G. Fox, *J. Atmos. Sci.* **29,** 322 (1972).
12. D. J. Shlien, *Physics Fluids* **21,** 2154 (1978).
13. D. J. Shlien, *Physics Fluids* **22,** 2277 (1979).

APPENDIX

THERMAL DIFFUSION

The spiral structure which can be considered almost a characteristic of vortex rings is seen in dyed vortex ring photos, e.g. [9] and [10] and in the shadowgraph of the sodium carbonate solution starting plume cap (Fig. 1) but is not visible in shadowgraphs of starting plume caps in water nor is any evidence of the spiral (beyond the valley region) found in the temperature field measurements. The lack of appearance of the spiral in the dilute sodium chloride solution shadowgraphs in contrast with the concentrated sodium carbonate solution shadowgraph might be attributable to different variations of refractive index with temperature of the two solutions and/or due to the different Prandtl numbers of the solutions. In this Appendix, a crude (order-of-magnitude) analysis of the diffusion process will be carried out to gauge to what extent the spiral structure may be expected under the present experimental conditions.

Heat is spread by molecular diffusion. In this, the laminar case, there is no 'mixing' to enhance the diffusion process; however the velocity gradients present tend to maintain temperature gradients. In this order-of-magnitude analysis only the thermal diffusion process is considered.

The time for one revolution of the spiral, a convection time, and the total number of spiral revolutions will be estimated. Time scales characteristic of the diffusion process will be estimated and compared with the times available for diffusion. Two regions will be considered which will give bounds on the diffusion process: (a) the spiral center, allowing the maximum time for diffusion and the shortest length scale over which the diffusion takes place; and (b) the entrainment (valley) region or outermost layer of the spiral allowing the shortest time for diffusion and the longest length scale.

(a) *Revolution time*

The time for one revolution of the spiral, τ_r is to be estimated by considering the difference in the fluid velocity on the axis and the fluid velocity at the rotational center. The former is less than or equal to the steady plume convection velocity while the latter is v_c, the cap convection velocity. The distance between the axis and the rotational center is r_0 and thus $\tau_r \cong 2\pi r_0/(v_p - v_c)$. However it has been observed [4] that $v_p \cong 2v_c$ so that $\tau_r \cong 2\pi r_0/v_c$. In this case $v_c = 25$ mm/s and $r_0 = 4.1$ mm, thus $\tau_r \cong 1.0$ s. It is to be noted that this is only a crude estimate.

(b) *Convection times*

(1) *Spiral center.* From the time sequence of dye photos of the vortex ring formation and development [9, 10], it is apparent that the spiral center originates at the time of formation of the cap. Thus the convection time for a fluid element located at the spiral center τ_0, should be equal to the total convection time of the cap. The quantity τ_0 may be estimated from previous measurements [13] to be 2.6 s.

(2) *Entrainment Region.* For the entraining region, an estimate of the velocity at which the ambient fluid is entrained is needed. This will be taken as the mean between the velocity on the axis v_a and the velocity of the convecting rotational center v_c where $v_a \cong v_p \cong 2v_c$. Thus, relative to the rising cap, ambient fluid is entrained at a velocity of $v_c/2 \cong 13$ mm/s. The overall height of the cap is 12 mm and thus the maximum convection distance is approximately 10 mm. Therefore the convection time of the entrained fluid, $\tau_c \cong 10/13 = 0.8$ s.

(c) *Number of spiral revolutions*

Since the spiral revolution time is 1.0 s and $\tau_0 = 2.6$ s, then the number of spiral revolutions should be $2.6/1.0 = 2.6$. In the same manner, the number of revolutions for the sodium carbonate case of Fig. 1 is estimated as 2.5 revolutions, which can just be distinguished in the shadowgraph.

(d) *Diffusion time scales*

A diffusion time can be defined as $\tau_D = l^2/D$, where D is the thermal diffusivity, 0.142 mm^2/s and l is the length scale over which the diffusion takes place. It can be seen in Fig. 10 that the width of the layers in the spiral decreases as the spiral center is approached. From the photos in [9] and from the contours of the measured temperature field, this characteristic width of the fluid layer at the spiral center l is estimated to be approximately $r_0/10\pi$ resulting in $\tau_D \cong 0.1$ s. It is to be noted that this choice of l is very approximate and since $\tau_D \propto l^2$, τ_D can only be considered an order-of-magnitude estimate. For the valley (entrainment) region, the characteristic width of the valley is estimated as $l \cong r_0/2\pi$. Thus for this case $\tau_D = 3$ s.

(e) *Comparison of time scales and conclusions*

For the spiral center region the diffusion time scale, $\tau_D \cong 0.1$ s, is considerably shorter than the convection time, $\tau_0 \cong 2.6$ s. Thus, even though the spiral is composed of an estimated 2.6 revolutions, the temperature distribution near the spiral center is expected to be diffused.

For the entrainment region, the diffusion time scale, $\tau_D \cong 3$ s, is of the same order of magnitude as the convection time, $\tau_c \cong 0.8$ s. Thus this rough estimate is inconclusive as to the extent of penetration of ambient temperature fluid into the valley region.

MESURE DE CHAMP DE TEMPERATURE DANS UN PANACHE LAMINAIRE NAISSANT

Résumé — On mesure le champ de température dans un panache laminaire, axisymétrique en formation, à l'aide d'une technique interférométrique avec inversion d'Abel. Les mesures montrent que la colonne de fluide qui suit la coiffea à peu près la même distribution de température que pour le panache stationnaire, ce qui confirme un aspect du modèle de Turner pour le cas laminaire. Le pic de température sur l'axe existe comme pour le cas stationnaire, mais on observe en plus un pic hors de l'axe au milieu de la coiffe et un pic sur l'axe près du bord de la coiffe. Ce dernier pic résulte de l'entraînement du fluide ambiant tandis que l'autre est probablement associé à l'instabilité. Les gradients de température au voisinage de ce pic sont importants et estimés à 200°C/m.

TEMPERATURFELDMESSUNG BEIM ENTSTEHEN EINER LAMINAREN SCHLIERE

Zusammenfassung — Das Temperaturfeld einer entstehenden achsensymmetrischen laminaren Schliere wurde zum ersten Mal unter Verwendung einer interferometrischen Meßtechnik und Inversionsdatenkorrektur nach Abel gemessen. Die Messungen zeigten, daß die der Kuppe folgende Säule des aufsteigenden Fluids praktisch die gleiche Temperaturverteilung wie die stationäre Schliere besitzt, was einen Teil des Modells von Turner über die Kuppe einer entstehenden Schliere im laminaren Fall bestätigt. Neben dem Temperaturmaximum auf der Achse, das dem bei der stationären Schliere entspricht, wurde ein weiteres nicht auf der Achse liegendes Maximum in der Mitte der Kuppe und ein unerwartetes axiales Maximum an der Anströmkante der Kuppe beobachtet. Das ersterwähnte Maximum resultiert aus dem mitgeführten Umgebungsfluid, während das letztere ungeklärt ist, aber möglicherweise mit der früher beobachteten Instabilität zusammenhängt. Temperaturgradienten in der Nähe dieses Maximums werden in der Größenordnung von 200°C/cm geschätzt.

ИЗМЕРЕНИЕ ТЕМПЕРАТУРНОГО ПОЛЯ В ЛАМИНАРНОЙ СВОБОДНО-КОНВЕКТИВНОЙ СТРУЕ

Аннотация — Приводятся результаты измерения температурного поля осесимметричной ламинарной свободно-конвективной струи в начале её формирования с использованием метода Абеля обработки интерферограмм. Измерения показали, что столб всплывающей жидкости вблизи насадка имеет почти то же распределение температуры, что и стационарная свободно-конвективная струя, что соответствует модели Тернера для начального участка ламинарной свободно-конвективной струи. Кроме максимума температуры на оси, соответствующего установившейся струе, наблюдался максимум вне оси в середине сопла и неожиданный максимум возле среза сопла. Первый из максимумов является результатом эжекции покоящейся жидкости, а наличие последнего, возможно, связано с неустойчивостью струи. Градиенты температуры вблизи этого максимума достигают 200 °C/см.